

Imaging of conductivity changes and electrode movement in EIT

Manuchehr Soleimani¹, Camille Gómez-Laberge² and Andy Adler²

¹ William Lee Innovation Centre, School of Materials, University of Manchester, UK

² School of Information Technology and Engineering (SITE), University of Ottawa, Canada

E-mail: M.Soleimani-2@manchester.ac.uk,{cgomez,adler}@site.uOttawa.ca

Abstract. Electrical Impedance Tomography (EIT) attempts to reconstruct the internal impedance distribution in a medium from electrical measurements at electrodes on the medium surface. One key difficulty with EIT measurements is due to the position uncertainty of the electrodes, especially for medical applications, in which the body surface moves during breathing and posture change. In this paper, we develop a new approach which directly reconstructs both electrode movements and internal conductivity changes for difference EIT. The reconstruction problem is formulated in terms of a regularized inverse, using an augmented Jacobian, sensitive to impedance change and electrode movement. A reconstruction prior term is computed to impose a smoothness constraint on both the spatial distribution of impedance change and electrode movement. A one-step regularized imaging algorithm is then implemented based on the augmented Jacobian and smoothness constraint. Images were reconstructed using the algorithm of this paper with data from simulated 2D and 3D conductivity changes and electrode movements, and from saline phantom measurements. Results showed good reconstruction of the actual electrode movements, as well as a dramatic reduction in image artefacts compared to images from the standard algorithm, which did not account for electrode movement.

Keywords: Electrical Impedance Tomography, regularization, image reconstruction, electrode movement.

1. Introduction

Electrical Impedance Tomography (EIT) attempts to reconstruct the internal impedance distribution in a medium from electrical measurements at electrodes on the medium surface. Since EIT is non-invasive, minimally cumbersome in terms of instrumentation, and potentially relatively inexpensive, it presents significant interest for medical and industrial applications for measuring or monitoring movement of conductivity contrasting substances. Medical applications of EIT include the monitoring of breathing and heart activity in the chest (Frerichs, 2000). Since the beginnings of EIT research, it has been recognized that electrode position uncertainty is a key source of errors and

artefacts in EIT images (Barber and Brown, 1988). In order to partially address this issue, EIT difference imaging has been used to reconstruct changes in the impedance distribution due to changes in measurements. Barber and Brown (1988) showed that difference imaging is much less sensitive to electrode position uncertainty when the electrodes do not move between measurements. Unfortunately, it is clear that, for many applications of EIT, the electrodes do move. In medical applications, electrode movement due to chest expansion during breathing and to changes in posture has a significant affect on measurements (Harris *et al* 1988, Adler *et al* 1996b, Zhang and Patterson 2005, Coulombe *et al* 2005).

Ideally, in a situation where electrodes move, it would be possible to calculate both the impedance distribution and the electrode locations. Lionheart (1998) showed that, for isotropic conductivity distributions in three dimensions, such a calculation is theoretically possible. Several groups have proposed algorithms to reconstruct electrode locations or boundary shape (Kiber *et al* 1990, Blott *et al* 1998, and Kolehmainen *et al* 2006). These approaches model the boundary shape in two dimensions, and iteratively fit the model parameters to the data. This paper develops a new algorithm to reconstruct both electrode movements and impedance changes from difference EIT data. The reconstruction problem is formulated in terms of a regularized inverse, in which an augmented Jacobian, sensitive to impedance change and electrode position, is computed. Results are shown for simulation and saline phantom data.

2. Methods

In this section, we develop a reconstruction algorithm to calculate both the impedance change and electrode movement for difference EIT. The algorithm is based on a finite element model (FEM) of a conductive medium discretized into n_N elements onto which n_E electrodes are attached on the FEM boundary. A current injection and measurement protocol is applied to obtain n_M measurements, referred to as a data *frame*. In our simulations and phantom experiments, an adjacent stimulation protocol is used, excluding measurements at stimulation electrodes. For a single ring of electrodes, $n_E = 16$, yielding $n_M = 208$ measurements per frame, while in three dimensions with two rings, $n_E = 32$, yielding $n_M = 928$.

2.1. System model

For difference EIT, frames \mathbf{v}_{t_1} and \mathbf{v}_{t_2} (size $n_E \times 1$) are acquired at times t_1 and t_2 , respectively. Based on these frames, the difference data ($\mathbf{v}_{t_2} - \mathbf{v}_{t_1}$) are calculated and represented by a vector \mathbf{z} of size $n_M \times 1$. Using this notation, we have n_N FEM elements with conductivities σ_{t_1} and σ_{t_2} taken at times t_1 and t_2 .

Difference EIT assumes that the difference measurements are a function *only* of the conductivity change between frames; thus $\Delta\sigma = \sigma_{t_2} - \sigma_{t_1}$. We use both point electrode models (in two dimensions) and the complete electrode model (in three dimensions). In

each case, the electrodes are represented by one or more nodes on the FEM boundary. The movement of an electrode j between difference frames is described by the vector $\vec{r}_j = (x_{j,t_1} - x_{j,t_2}, y_{j,t_1} - y_{j,t_2}, z_{j,t_1} - z_{j,t_2})$, where (x_j, y_j, z_j) represents the average nodal co-ordinates of an electrode j at given measurement frame. If an electrode is modelled by several nodes (using the complete electrode model), all nodes are assumed to move identically. For large movements, such a modification of the FEM will produce artefacts due to the distorted shape of the simplices. However, for this algorithm, only small deformations of the FEM model are considered. Based on the difference measurements, \mathbf{z} , we attempt to reconstruct an *image* $\hat{\mathbf{x}}$ of size $(n_N + 3n_E) \times 1$, which represents the conductivity variations and the electrode movements between frames. The first n_N entries represent the conductivity variation $\Delta\sigma$ for each element. The remaining $3n_E$ entries are the electrode movements, \vec{r}_j , for each electrode. In two dimensions there are two cartesian axes, and $\hat{\mathbf{x}}$ has size $(n_N + 2n_E) \times 1$.

2.2. Forward calculations

We represent the forward solution as the computation of difference measurements \mathbf{z} from the conductivity change and electrode movement, \mathbf{x} , by the EIT difference operator F , based on the FEM, relative to an assumed homogeneous distribution σ_h at t_1 . That is,

$$\mathbf{z} = F(\mathbf{x})|_{\sigma_h} \quad (1)$$

The image reconstruction is formulated by a regularized *maximum a posteriori* framework using Gaussian priors (Adler and Guardo, 1996). The reconstructed image is

$$\hat{\mathbf{x}} = \arg \min_{\mathbf{x}} (\mathbf{z} - F(\mathbf{x}))^t \Sigma_n^{-1} (\mathbf{z} - F(\mathbf{x})) + (\mathbf{x} - \mathbf{x}_\infty)^t \Sigma_x^{-1} (\mathbf{x} - \mathbf{x}_\infty) \quad (2)$$

where \mathbf{x}_∞ represents the expected value of element conductivity changes and electrode motion. We assume that the conductivity changes and electrode motion may be equally positive or negative, and set $\mathbf{x}_\infty = 0$ for our calculations in this paper. The matrices Σ_x and Σ_n are the *a priori* estimates of the image (augmented by electrode movement data) and measurement noise covariance matrices, such that each element $[\Sigma_x]_{i,j}$ represents $cov(\mathbf{x}_i, \mathbf{x}_j)$.

We do not calculate these covariances directly, but rather develop matrices \mathbf{W} and \mathbf{R} to represent Σ_n^{-1} and Σ_x^{-1} . Given an average measurement noise amplitude σ_n , \mathbf{W} is defined as

$$\frac{1}{\sigma_n^2} \mathbf{W} = \Sigma_n^{-1} \quad (3)$$

where $\mathbf{W}_{i,i}$ represents the inverse of the relative noise power for measurement i . To simplify our analysis, the all measurements are considered to have equal noise, giving $\mathbf{W} = \mathbf{I}$. A more sophisticated model would be necessary if a specific EIT system varies the gain, and thus the noise level, in each channel.

The upper $n_N \times n_N$ part of Σ_x^{-1} represents the covariance between finite element conductivity changes, while the lower $n_D n_E \times n_D n_E$ part represents the covariance

between electrode movements, where n_D is the model dimension (2D or 3D). We assume that there is no correlation between electrode movement and conductivity changes. For specific applications of EIT, such as for lung imaging, one would expect electrode movement and conductivity changes to be correlated. However, to impose such prior information on the algorithm may introduce artefacts into reconstructed images when such correlations do not hold. Based on these assumptions, we model the image covariance as

$$\Sigma_x^{-1} = \frac{1}{\sigma_c^2} \mathbf{R}_c + \frac{1}{\sigma_m^2} \mathbf{R}_m \quad (4)$$

where σ_c and σ_m represent the *a priori* amplitude of conductivity change and electrode movement, respectively. \mathbf{R}_c is the regularization matrix for conductivity change, and is non-zero in the upper $n_N \times n_N$ values. Similarly, \mathbf{R}_m is the regularization matrix for electrode movement, and is non-zero in the lower $n_D n_E \times n_D n_E$ elements.

In order to model the expected smoothness of real conductivity change patterns, \mathbf{R}_c should be a spatial high pass filter (Adler and Guardo, 1996). We model the inter-element correlations using a discrete Laplacian filter, so that the diagonal elements $[\mathbf{R}_c]_{i,i} = n_D + 1$. The off-diagonal elements $[\mathbf{R}_c]_{i,j}$ are set to -1 if finite elements i and j are adjacent (i.e. share at least n_D nodes), and are otherwise set to zero. Within the electrode movement model \mathbf{R}_m , it is again reasonable to expect a non-zero inter-element correlation, as adjacent electrodes may be expected to move similarly. In a similar way to the conductivity change parameters, we model inter-element correlations using a discrete Laplacian, so that the diagonal elements $[\mathbf{R}_m]_{i,i} = 2.1$. The off-diagonal elements $[\mathbf{R}_m]_{i,j}$ are set to -1 for adjacent electrodes i and j , and if not are set to zero. We choose $[\mathbf{R}_m]_{i,i} = 2.1$ rather than 2 in order to impose a non-zero penalty for global movement of all electrodes.

Parameters σ_c and σ_m model the expected magnitude of the conductivity changes and electrode movements, and may have dramatically different values, since they are measured in different units. We define $\mu = \sigma_c/\sigma_m$ as the model hyperparameter to represent the compromise between model fidelity to conductivity changes or movements. In order to estimate a range for μ , we note that for medical applications of EIT, such as breathing, conductivity changes on the order of the magnitude of $1.0 \times \sigma_h$ may be expected, while electrode movements may be 5% of the medium diameter. Thus, we estimate values of $\mu = 1/0.05 = 20$, to be reasonable. Figures 1 illustrates the effect of variations in μ .

2.3. Inverse calculations

The inverse calculations are modified to account for electrode movement. The movement portion of the Jacobian is calculated using a perturbation method, where the i, j th element of the Jacobian \mathbf{J} represents the ratio of a change in measurement i for a small change in finite element j .

$$\mathbf{J}_{i,j} = \frac{F_i(\mathbf{x}_j + \Delta \mathbf{x}_j)}{\Delta \mathbf{x}_j} \quad (5)$$

where $\Delta \mathbf{x}_j$ is chosen to be sufficiently large to avoid numerical errors, but small enough that it accurately approximates the Jacobian. In order to validate the choice of $\Delta \mathbf{x}_j$, we evaluated the change in \mathbf{J} as a function of $\Delta \mathbf{x}$. For calculations with double precision arithmetic, the relative variation in \mathbf{J} is less than 10^{-6} for $\Delta \mathbf{x} = 10^{-6}$. Based on the calculated Jacobian, we use the linear approximation, $F(\mathbf{x}) = \mathbf{J}\mathbf{x}$. Thus (2) may be interpreted as a one step linear inverse solution (Cheney *et al* 1990) for the conductivity and electrode movement $\hat{\mathbf{x}}$ based on data \mathbf{z}

$$\hat{\mathbf{x}} = \left(\mathbf{J}^t \frac{1}{\sigma_n^2} \mathbf{W}\mathbf{J} + \frac{1}{\sigma_c^2} \mathbf{R}_c + \frac{1}{\sigma_m^2} \mathbf{R}_m \right)^{-1} \mathbf{J}^t \frac{1}{\sigma_n^2} \mathbf{W}\mathbf{z}. \quad (6)$$

We define $\mathbf{R} = \mathbf{R}_c + \mu^2 \mathbf{R}_m$, and rewrite (6) as (using $\mathbf{W} = \mathbf{I}$),

$$\hat{\mathbf{x}} = (\mathbf{J}^t \mathbf{J} + \lambda^2 \mathbf{R})^{-1} \mathbf{J}^T \mathbf{z}. \quad (7)$$

where λ^2 is the global regularization hyperparameter, such that $\lambda = \sigma_n / \sigma_c$. Elements in the lower part of \mathbf{R} are now scaled by $\sigma_c^2 / \sigma_m^2 = \mu^2$. Thus, \mathbf{R} is represented by

$$\mathbf{R}_{i,j} = \begin{cases} n_D + 1 & \text{if } i = j \text{ and } i \leq n_N \\ -1 & \text{if (element } i \text{ is adjacent to } j \text{) and } (i \leq n_N) \\ 2.1\mu^2 & \text{if } i = j \text{ and } i > n_N \\ -\mu^2 & \text{if (electrode } i \text{ is adjacent to } j \text{) and } (i > n_N) \\ 0 & \text{otherwise.} \end{cases} \quad (8)$$

2.4. Standard method

In order to compare our results to those calculated without compensation for electrode movement, we develop a reconstruction model based solely on the conductivity change part of \mathbf{J} and \mathbf{R} . This corresponds to a one step EIT reconstruction similar to that of Cheney (1990) or Adler and Guardo (1996). In our results we refer to this technique as the *standard method*.

2.5. Artefact amplitude measure

Images reconstructed with compensation for electrode movement appear to show reduced reconstruction artefacts in comparison with the standard method. To measure this effect, we define an measure of reconstruction artefact amplitude (AAM) as follows. A reconstruction artefact is defined to be an element of non-zero conductivity change in elements which we know (from the physical or simulation model) to have zero conductivity change. AAM, is defined to be

$$\text{AAM} = \sqrt{\frac{\sum_{i \in L} A_i \mathbf{x}_i^2}{\sum_{i \in L} A_i}} \quad (9)$$

where A_i is the area (in 2D) or volume (in 3D) of each element, and L is the set of elements selected. For simulated results, L includes all elements which do not overlap with any contrast element in the forward model. For measured phantom data, L is defined to include elements in the two rings of finite elements closest to the boundary.

2.6. Experimental data

Test data were calculated both by numerical simulation and experimentation using a saline tank phantom. Numerical simulations were conducted using planar and volumetric FEM models with 576 elements in two dimensions and 828 elements in three dimensions using the EIDORS software (Adler and Lionheart, 2006). The 2D simulation model differs from that used to reconstruct images to avoid the *inverse crime*.

Saline phantom data were acquired from a 30 cm diameter and 30 cm tall plastic cylindrical phantom filled with 0.9% saline solution to the 20 cm mark. Sixteen stainless steel electrodes were placed, equally spaced, around the circumference at a vertical position of 10 cm above the base of the tank. EIT data were acquired using the Goe-MF II EIT system (Viasys Healthcare, Höchberg, Germany) using an adjacent stimulation and measurement pattern. Homogeneous data \mathbf{z}_h were first acquired, and subsequently, small non-conductive spherical objects of 2 cm radius were introduced in the plane of the electrodes at various positions along the x and y axes. Electrode movement was simulated by applying an elliptical deformation to the phantom such that the diameter of the top of the phantom on the x -axis was reduced by 5 cm. The electrode channel impedances were tested to be between 200 and 400 Ohms according to the system's calibration test. These values are within the system's acceptable limits.

3. Results

This algorithm was implemented in Matlab (v.7 SP2) and tested using a 2.60 GHz AMD Opteron based computer under Linux. The calculation of the complete reconstruction of the three dimensional problem took 25.2 sec. while the computation of a single-step inverse required approximately 10 ms. This approach would thus be appropriate for real-time EIT imaging. The software developed has been contributed to the EIDORS project (Adler and Lionheart, 2006).

Simulated 2D data were generated using the circular model shown in the top left part of figure 1. \mathbf{v}_{t_1} was calculated for a homogeneous circular medium; \mathbf{v}_{t_2} was calculated for a medium with two small inhomogeneities of conductivity $1.2 \times \sigma_h$ and $0.8 \times \sigma_h$, where the boundary was distorted into an elliptical shape, with a 1% elongation vertically and a 1% compression horizontally. Noise was added to measurements to give a signal-to-noise ratio (SNR) of 20 dB, with the signal defined as $\|\mathbf{z}\|^2$. The top right part of figure 1 is an image reconstructed from these data using the standard method with $\lambda = 10^{-2}$. The images reconstructed using the standard method show a large level of artefacts around the medium boundary, as well as an incorrect position for the reconstructed contrasts, which appear to be "pushed" in the direction of boundary movement. Images reconstructed using the proposed algorithm (figure 1 bottom row) show dramatically reduced artefacts, as well as more accurate positioning of contrasts. When μ is small, the penalty for movements is low, and the algorithm is able to make arbitrary electrode movements to satisfy the conductivity change constraints (bottom

left of figure 1 shows $\mu = 1$). Using a more reasonable value, $\mu = 20$, the image (bottom right) shows reasonable reconstructed movement and conductivity change.

Reconstructed images for phantom data are shown in figure 2. The phantom was compressed along the x -axis by 5 cm at the top of the tank. Since electrodes were placed at 1/3 of the tank height, each electrode moved by 6.7% of the tank radius. The contrasts were reconstructed at the correct locations, in both the proposed and standard algorithms, although artefacts in the standard method (left) are significantly larger.

In order to test this method on volumetric reconstructions, simulations were calculated using the 828 element mesh of figure 3. Difference data were calculated

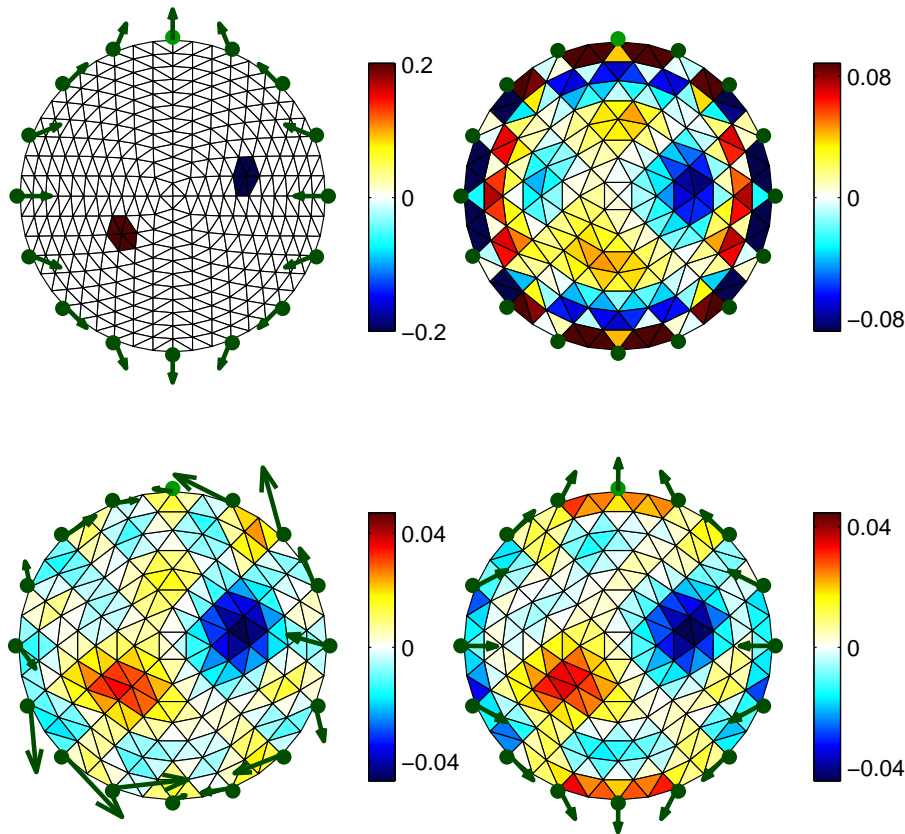


Figure 1. Simulated images of reconstructed conductivity and electrode movement. Arrows indicate each electrode's movement, and are scaled by $20\times$. *Top left:* FEM (576 element mesh) for 2D simulation of conductivity change and electrode movement from an elliptical deformation of 1% of medium diameter. Noise of 20 dB SNR is added to simulated data. *Top right:* Reconstructed image (256 element mesh) using the standard method with $\lambda = 10^{-2}$ (Artefact amplitude AAM = 0.0616). *Bottom left:* Reconstructed image including electrode movement with $\lambda = 10^{-2}$ and $\mu = 1$ (AAM = 0.0116). *Bottom right:* Reconstructed image including electrode movement using $\lambda = 10^{-2}$ and $\mu = 20$ (AAM = 0.0135).

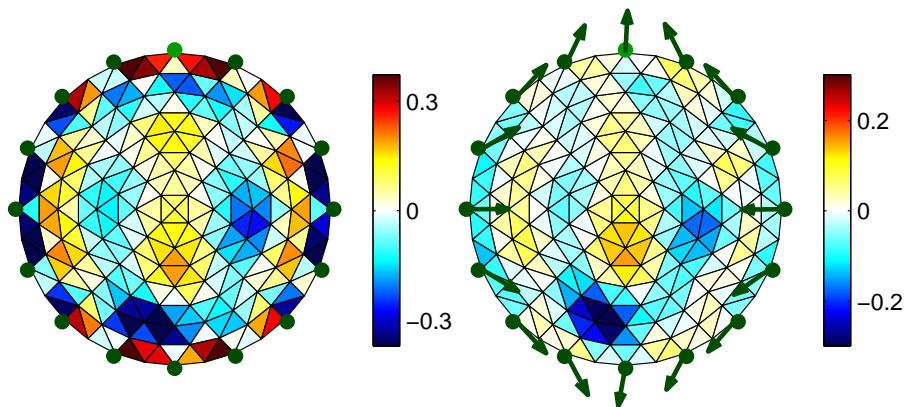


Figure 2. Reconstructed images (256 element mesh) for phantom data with two non-conductive objects: one on the positive x -axis, the other on the negative y -axis. Arrows indicate each electrode's movement, and are scaled by $10\times$. *Left:* Reconstructed image with standard method using $\lambda = 10^{-2}$ (AAM = 0.134). *Right:* Reconstructed image including electrode movement using $\lambda = 10^{-2}$ and $\mu = 10$ (AAM = 0.0273).

due to the introduction of conductive and non-conductive contrasts, and a complex 3D distortion in the x and y axes. Images reconstructed from this mesh are shown in figure 4, using the standard method and the proposed algorithm. As in the case of 2D reconstructions, the proposed algorithm is able to calculate reasonably accurate electrode movements, and is also able to significantly reduce the level of reconstruction artefacts do to electrode movement.

4. Discussion

One of the main challenges in applications of EIT is compensating for image artefacts due to uncertainty of electrode position. This paper proposes an algorithm, based on our previous work (Soleimani *et al* 2003, 2004) to reconstruct both the conductivity change and electrode movement from difference EIT data. This method was tested on simulated and experimental phantom data in planar and volumetric media, and showed an ability to accurately reconstruct images in all cases. The direction of electrode movement was correctly calculated for both simulated and experimental data. Additionally, if only the conductivity change portion of the image is of interest, then this algorithm allows reconstruction of images with dramatically reduced artefacts in the presence of electrode movement.

From very early days in EIT research, it has been observed that electrode movement is a significant source of errors and artefacts in images. This is a particularly difficult issue in static EIT imaging, as illustrated by Barber and Brown (1988) who showed that difference imaging is relatively immune to electrode position errors which do not vary between measurements. Gersing *et al* (1996) measured the effect of changes in

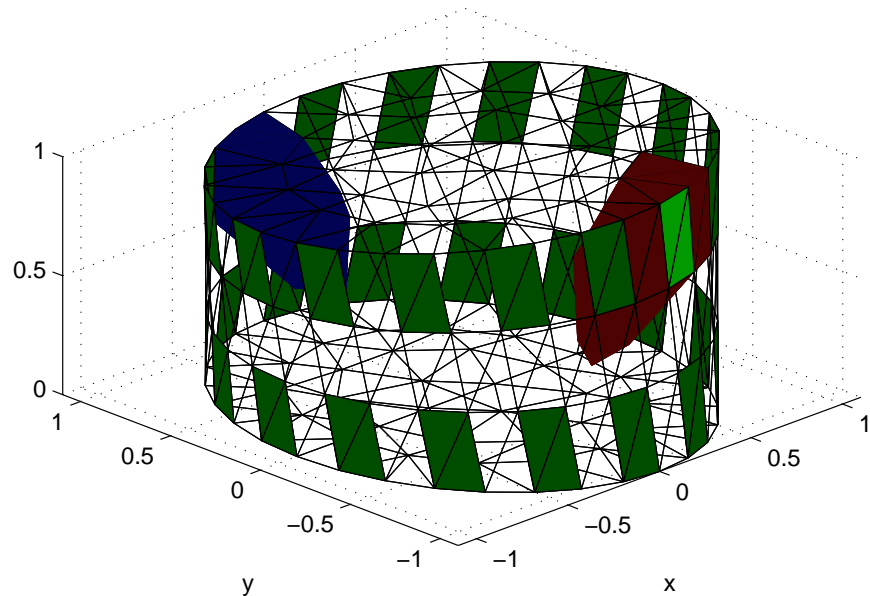


Figure 3. Volumetric model with a geometrical distortion applied (exaggerated 10 times to clarify the geometry). The mesh has 828 tetrahedral elements and two rings of 16 electrodes. Blue and red regions indicate contrasts being less conductive and more conductive, respectively, than the surrounding medium.

medium geometry on EIT measurements, and Kolehmainen *et al* (1997) simulated the effect of errors in the boundary model for static imaging using an elliptical deformation of a circular boundary, and showed significant errors for boundary model deformations of 1%. Another approach has been to measure the electrode positions, using a system such as that of Molebny *et al* (1996).

For EIT images of the thorax, the primary causes of electrode movement are due to posture changes and breathing. The effect of postural changes on EIT measurements has been studied by Harris *et al* (1988), Lozano *et al* (1995), and Coulombe *et al* (2005). In each case, participants were asked to assume different postures and significant differences in EIT images were observed. Interestingly, Harris *et al* (1998) suggest that this result may be due to changes in distribution of ventilation with posture; however, we feel it is more likely that electrode movement is the most significant effect (as shown by recent stimulation studies, such as Zhang and Patterson, 2005). Electrode movement with breathing is caused by the expansion of the rib cage (Frerichs, 2000). Simulation studies of the this effect have been conducted by Adler *et al* (1996b) and Zhang and Patterson (2005). Finite element models of the chest were constructed and EIT measurements

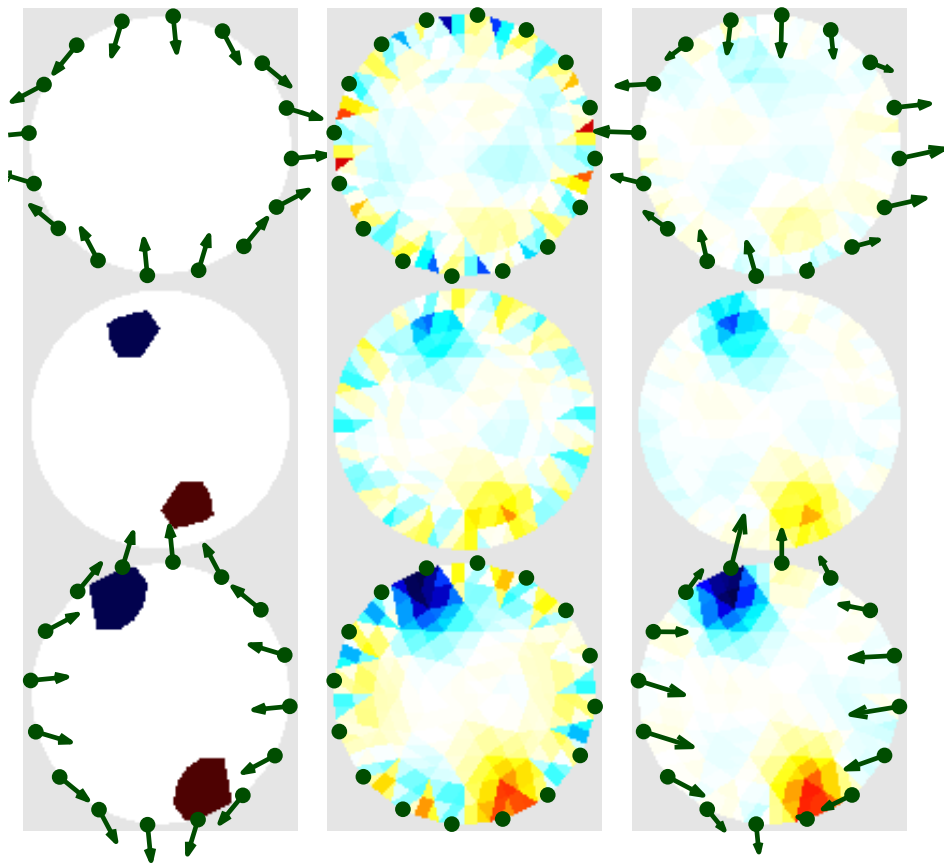


Figure 4. Reconstructed images and electrode movement from simulated volumetric data with 20 dB SNR noise, using hyperparameters $\lambda = 3 \times 10^{-3}$ and $\mu = 20$. Each column shows three horizontal slices of the reconstructed image on a 828 element mesh (top: $z = 0.167$; middle: $z = 0.500$; bottom: $z = 0.833$). Electrodes are indicated by a dot at the centre of the electrode position. Arrows indicate each electrode's movement, and are scaled by $10\times$. *Left*: Simulated inhomogeneities and electrode movements. *Middle*: Reconstructed image using the standard algorithm (AAM = 0.0708). *Right*: Reconstructed image including electrode movement (AAM = 0.0190).

simulated due to changes in lung conductivity and electrode movement with breathing. Both studies reported a broad central image artefact whose amplitude was proportional to the EIT image due to the conductivity change.

Several groups have attempted to model the boundary shape from EIT measurements. This possibility was first observed by Breckon and Pidcock (1988), who suggested fitting a Fourier series approximation to the boundary shape. Kiber *et al* (1990) showed a way to estimate the shape of the boundary from electrical data using a two-dimensional model, and reported good results for an elliptical tank and some success on data from a thorax. Blott *et al* (1998), and Kolehmainen *et al* (2006) developed algorithms to compensate for electrode position variations, based on a perturbation of the Jacobian similar to that presented here. A regularized expression was developed

and iteratively solved based on the conductivity changes and electrode movements. This work differs from ours in that the electrode movements are not directly modelled as spatial coordinates, and the relative choice of regularization hyperparameters for movement and conductivity terms appears to be heuristic. Additionally, only two-dimensional simulations are presented.

An important theoretical result was given by Lionheart (1998), who showed that if the boundary shape is wrong (in a three-dimensional problem) there will not generally be an isotropic conductivity which fits the measured boundary data. Thus, in theory, both impedance and boundary shape can be calculated from EIT data. For two-dimensional models, isotropic conductivity and boundary shape can be recovered up to a conformal mapping relation. The applicability of this result to this study is limited by the fact that we consider difference EIT data, and a limited number of electrodes, rather than complete boundary data.

Many researchers have considered the problem of reconstructing the shape of targets in a medium with a fixed boundary (Han and Prosperetti 1999, Heikkinen *et al* 2002, Kolehmainen *et al* 2001, Tossavainen *et al* 2004, Vauhkonen *et al* 1998). Techniques to model internal boundaries are probably more advanced than those to model the medium boundary and electrode positions. For example, Kolehmainen *et al* (2001) formulates the inverse problem in terms of state space estimation and computes the parameters using the extended Kalman filter. Such techniques, which consider the temporal characteristics of the data, are almost certainly applicable to the medium boundary problem considered here.

In addition to electrode movement, changes of electrode contact impedance are a significant issue in EIT applications, especially for monitoring applications (Lozano *et al* 1997). While we do not address this issue in this paper, it is interesting to note the approach taken by Heikkinen *et al* (2002) to address simultaneous reconstruction of the impedance distribution and electrode contact impedances. Similar to the approach taken here, a composite Jacobian is calculated, based on changes in both parameters. One potentially useful advancement would be a development of the approach proposed here to also consider electrode impedance in this way. Additionally, it may be possible to reconstruct the overall distortion of the boundary as well as the movement of the electrodes. In this study, we include phantom experiments to test our proposed algorithm. Electrode movements are a difficult problem to simulate and we felt that a demonstration of experimental results is necessary to ensure our method is not only applicable to simulated data.

One limitation of our study is the use of fixed electrode models, in which all nodes for each electrode translate uniformly, without distortion or rotation. However, real electrode displacements are far more complex. The electrode will turn as it moves, the skin under it will buckle, and the electrode itself may deform. It is possible that the difference noted between reconstructions from simulations and from phantom data reflects some of this difference.

In conclusion, we have developed an algorithm to reconstruct conductivity change

and electrode movement in EIT. Results show good reconstructions for both simulated and phantom measurements. The electrode movement is faithfully reconstructed, and the conductivity change shows dramatically less artefacts than for standard methods. One key advantage is that, once pre-calculations are done, it requires little additional computational time over standard methods. We anticipate that these techniques may be useful to increase the accuracy and reliability of EIT in clinical and experimental applications.

Acknowledgments

This work was supported by a grant from the Natural Sciences and Engineering Research Council of Canada.

References

- Adler A and Lionheart W R B 2006 Uses and abuses of EIDORS: An extensible software base for EIT *Physiol. Meas.*, in press.
- Adler A and Guardo R 1996 Electrical impedance tomography: regularized imaging and contrast detection *IEEE Trans. Med. Imaging* **15** 170–9
- Adler A Guardo R and Berthiaume Y 1996b Impedance imaging of lung ventilation: Do we need to account for chest expansion? *IEEE Trans. Biomed. Eng.* **43**(4) 414–20
- Barber D C and Brown B H 1988 Errors in reconstruction of resistivity images using a linear reconstruction technique *Clin. Phys. Physiol. Meas.* **9**(suppl. A) 101–4
- Blott B H Daniell G J and Meeson S 1998 Electrical impedance tomography with compensation for electrode positioning variations *Phys. Med. Biol.* **43** 1731–9
- Breckon W and Pidcock M 1988 Data errors and reconstruction algorithms in electrical impedance tomography *Clin. Phys. Physiol. Meas.* **9**(suppl. A) 105–9
- Cheney M Isaacson D Newell J C Simske C and Goble J C 1990 NOSER: An algorithm for solving the inverse conductivity problem *Int. J. Imaging Systems & Technol.* **2** 66–75
- Coulombe N Gagnon H Marquis F Skrobik Y and Guardo R 2005 A parametric model of the relationship between EIT and total lung volume *Physiol. Meas.* **26** 401–11
- Frerichs I 2000 Electrical impedance tomography (EIT) in applications related to lung and ventilation: a review of experimental and clinical activities *Physiol. Meas.* **21** R1–21
- Gersing E Hoffman B and Osypka M 1996 Influence of changing peripheral geometry on electrical impedance tomography measurements *Med. Biol. Eng. Comput.* **34** 359–61
- Han D D K and Prosperetti A 1999 A Shape Decomposition Technique in Electrical Impedance Tomography *J. Comput. Physics* **155** 75–95
- Harris N D Suggett A J Barber D C and Brown B H 1988 Applied potential tomography: a new technique for monitoring pulmonary function *Clin. Phys. Physiol. Meas.* **9** 79–85
- Heikkinen L M Vilhunen T West R M and Vauhkonen M 2002 Simultaneous reconstruction of electrode contact impedances and internal electrical properties, Part II: Applications *Meas. Sci. Technol.* **13** 1855–61
- Kiber A Barber D C and Brown B H 1990 Estimation of Object Boundary Shape from the Voltage Gradient Measurements *Proc. Meet. on Electrical Impedance Tomography (Copenhagen)* ed. T K Hames pp 52–9
- Kolehmainen V Vauhkonen M Karjalainen P A and Kaipio J P 1997 Assessment of errors in static electrical impedance tomography with adjacent and trigonometric current patterns *Physiol. Meas.* **18** 289–303

- Kolehmainen V Voutilainen A and Kaipio J P 2001 Estimation of non-stationary region boundaries in EIT - State estimation approach *Inverse Problems* **17** 1937–56
- Kolehmainen V Lassas M and Ola P 2006 Inverse conductivity problem with an imperfectly known boundary *SIAM J. Appl. Math.* **66**(2) 365–383
- Lionheart W R B 1998 Boundary Shape and Electrical Impedance Tomography *Inverse Problems* **14** 139–47
- Lozano A Rosell J Pallás-Areny R 1995 Errors in prolonged electrical impedance measurements due to electrode repositioning and postural changes *Physiol. Meas.* **16** 121–30
- Lozano A 1997 Electrode Errors in bioimpedance measurements for long-term applications *Proc. 16th Southern Biomed. Eng. Conf.* Biloxi, MS, USA
- Molebny V V Lionheart W R B Vovk P P Mykytenko Y H and Gouz V I 1996 Sensor Position Measurement for Electroimpedance Tomography *Med. & Biol. Eng. Comput.* **34**(1) 177–8
- Soleimani M Abascal J F P J and Lionheart W R B 2004 Simultaneous reconstruction of the boundary shape and conductivity in 3D electrical impedance tomography *Proc. XII. Int. Conf. on Electrical Bio-Impedance V. Electrical Impedance Tomography* Gdansk, Poland, pp 475–8
- Soleimani M Sadleir R and Jersey-Willuhn K 2003 Simultaneous reconstruction of the boundary shape and conductivity in 2D electrical impedance tomography *Proc. 3rd World Congress on Industrial Process Tomography* Banff, Alberta, Canada, pp 695–700
- Tossavainen O-P Vauhkonen M Heikkinen L M and Savolainen T 2004 Estimating shapes and free surfaces with electrical impedance tomography *Meas. Sci. Technol.* **15** 1402–11
- Vauhkonen M Karjalainen P A and Kaipio J P 1998 A Kalman filter approach applied to the tracking of fast organ boundaries *Proc. IEEE Eng. Med. Biol. Soc.* **20**(2) 1048–51
- Zhang J and Patterson R P 2005 EIT images of ventilation: what contributes to the resistivity changes? *Physiol. Meas.* **26** S81–S92